AD-A092 737 CINCINNATI UNIV OH DEPT OF AEROSPACE ENGINEERING AND--ETC F/G 20/4
THREE DIMENSIONAL INTERNAL FLOWS IN TURBOMACHINERY. VOLUME I.(U)
JUN 80 A A HAMED F49620-78-C-0041

UNCLASSIFIED AFOSR-TR-80-1214 NL

1 of 1
AD
A092737

END
DATE
FILMED
1 81
DTIC

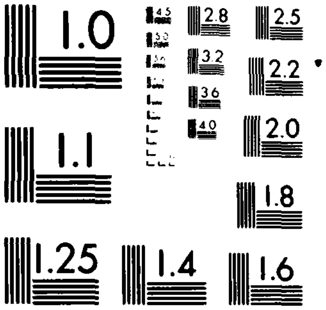

MICROCOPY RESOLUTION TEST CHART
NATIONAL BUREAU OF STANDARDS 1963-A

AFOSR-TR- 80-1214

LEVEL

12

AD A092737

THREE DIMENSIONAL INTERNAL FLOWS
IN TURBOMACHINERY
VOLUME I

FINAL REPORT
ON
AFOSR CONTRACT F49620-78-C-0041

DTIC
DEC 10 1980
C

January 1978 to June 1980

Principal Investigator: Awatef A. Hamed

DDC FILE COPY

Approved for public release;
distribution unlimited.

80 12 08 07

SECURITY CLASSIFICATION UNCLASSIFIED

(19) REPORT DOCUMENTATION PAGE

READ INSTRUCTIONS BEFORE COMPLETING FORM

1. REPORT NUMBER (18) AFOSR-TR- 80-1214

2. GOVT ACCESSION NO. AD-A092737

3. RECIPIENT'S CATALOG NUMBER

4. TITLE (and Subtitle) (6) THREE DIMENSIONAL INTERNAL FLOWS IN TURBOMACHINERY. ~~Vol I~~ Volume I.

5. TYPE OF REPORT & PERIOD COVERED (9) FINAL rept. Jan 78-Jun 80

6. PERFORMING ORG. REPORT NUMBER

7. AUTHOR(s) (10) AWATEF A. HAMED

8. CONTRACT OR GRANT NUMBER(s) (15) F49620-78-C-0041

9. PERFORMING ORGANIZATION NAME AND ADDRESS

UNIVERSITY OF CINCINNATI
DEPT OF AEROSPACE ENGINEERING & APPLIED ~~MATHEMATICS~~ Mechanics
CINCINNATI, OHIO 45221

10. PROGRAM ELEMENT, PROJECT, TASK AREA & WORK UNIT NUMBERS

61102F
(16) 2307 A1 (17) A1

11. CONTROLLING OFFICE NAME AND ADDRESS

AIR FORCE OFFICE OF SCIENTIFIC RESEARCH/NA
BOLLING AFB, DC 20332

12. REPORT DATE (11) Jun~~e 19~~80

13. NUMBER OF PAGES 45

14. MONITORING AGENCY NAME & ADDRESS (if different from Controlling Office) (12) 51

15. SECURITY CLASS. (of this report) UNCLASSIFIED

15a. DECLASSIFICATION/DOWNGRADING SCHEDULE

16. DISTRIBUTION STATEMENT (of this Report)

Approved for public release; distribution unlimited

17. DISTRIBUTION STATEMENT (of the abstract entered in Block 20, if different from Report)

18. SUPPLEMENTARY NOTES

19. KEY WORDS (Continue on reverse side if necessary and identify by block number)

SECONDARY FLOW
ROTATIONAL FLOW
THREE DIMENSIONAL FLOW
EXPERIMENTAL LDV FLOW MEASUREMENTS

20. ABSTRACT (Continue on reverse side if necessary and identify by block number)

This report describes an efficient numerical scheme developed for investigating secondary flows, and outlines the design of an experimental set-up for obtaining detail in channel three dimensional secondary flow measurements. The analysis applies to inviscid internal rotational flow fields and leads to a very efficient numerical scheme for predicting the secondary flow phenomena. The analysis is applied to the rotational flow in a 90° bend with rectangular cross-section and then compared with the experimental data. It is concluded

DD FORM 1 JAN 73 1473 EDITION OF 1 NOV 65 IS OBSOLETE

UNCLASSIFIED 411

SECURITY CLASSIFICATION OF THIS PAGE (When Data Entered)

is concluded from the comparison that the physics of the secondary flow problem are well represented in the analysis. The analysis can be adapted with some modifications to variable area ducts, and turbomachinery passages.

SUMMARY

This report describes an efficient numerical scheme developed for investigating secondary flows, and outlines the design of an experimental set-up for obtaining detail in channel three dimensional secondary flow measurements. The analysis applies to inviscid internal rotational flow fields and leads to a very efficient numerical scheme for predicting the secondary flow phenomena. The analysis is applied to the rotational flow in a 90° bend with rectangular cross-section and then compared with the experimental data. It is concluded from the comparison that the physics of the secondary flow problem are well represented in the analysis. The analysis can be adapted with some modifications to variable area ducts, and turbomachinery passages.

TABLE OF CONTENTS

Page

NOMENCLATURE

D_e-z	light beam diameter entering lense
d_f	fringe spacing
dm	diameter of laser beam in x direction at crossing point
f	focal length of focusing optics
F_D	frequency detected at photodetector
H	
K	half the angle of the dual beam intersection at the measuring point.
P	total pressure divided by density
R_i, R_o	inner and outer radiis of the duct.
u,v,w	velocity component in r, θ and z directions, respectively
$\bar{V}$	velocity vector

Greek Symbols

$\bar{\Omega}$	vorticity vector
η, ξ, ζ	vorticity components in r, θ and z directions, respectively
χ	streamlike function
λ	laser wave length
ϕ	the angle of laser beam intersection

Subscripts

i	inner
o	outer
I	inlet
max	maximum

PERSONNEL

The following personnel have contributed to this investigation:

W. Tabakoff, Professor of Aerospace Engineering and Applied Mechanics

S. Abdallah, Graduate Research Assistant

A. Darus, Graduate Research Assistant

Y. Sugiyama, Graduate Research Assistant

J. Cupito, Mechanic.

INTRODUCTION

The basic understanding of the secondary flow phenomenon and of ways to reduce the losses associated with it, is needed for the development of new high performance turbomachines. The main effect of the secondary flow on overall turbomachinery performance is a result of its influence on the angle and the energy distribution of the flow leaving the blade rows. A deviation in the existing flow angles from those predicted by the blade element analysis results from the secondary velocities. The secondary losses are also caused by the redistribution of the low energy flow by the same secondary velocities. These cross velocities are associated with the secondary vorticity development in the streamwise direction through the turning of the flow with nonuniform inlet conditions in the blade passages.

Secondary flow in compressor and turbine cascades has been the subject of several theoretical and experimental investigations. In most of the experimental secondary flow investigations, the flow measurements have been limited to cascade inlet and exit conditions to provide empirical correlations for secondary flow losses and exit flow angles [1, 2 and 3]. Although some experiments included blade surface static pressure measurements and some used visualization techniques at the end walls, no detailed in-channel experimental flow measurements are available to date. In the present study, an experimental set-up has been designed to provide detailed three dimensional in-channel secondary flow measurements. The main objectives of the design were to maintain high accuracy in the measurements of the secondary velocity without disturbing the secondary flow pattern, and to remove any ambiguity in the definition of the direction of these relatively small velocities. These objectives were maintained in the design of the tunnel, the Laser Doppler Velocimeter, the particle feeder for feeding the flow, the optical system and the data acquisition system. The details of the experimental set-up design and calculations, and a discussion of the methods for obtaining the secondary flow measurements can be found under the section on the experimental study.

Traditionally, the effect of secondary flow on cascade flow exit angle have been estimated analytically through the superposition of the secondary velocities on the irrotational flow field. These velocities are computed from approximate expressions of the secondary vorticity [4, 5]. Turbomachinery flow field solutions are usually based on synthesizing the three dimensional flow field from two dimensional computations on stream surfaces in the manner described by Wu [6]. The very few existing numerical inviscid secondary flow solutions [7 and 8] are based on the same approach. This limits these analyses to flows with small stream surface warpage, such as in compressor cascades, because of the small deflection in the flow channels. Horlock [9] pointed out the need for the development of a three dimensional analysis that can predict the excessive secondary rotations in the case of turbine blade rows. In the present study, a new analytical formulation for the secondary flow problem has been developed as reported in reference [10]. The primary objective in arriving at this formulation was that it should not be limited to small stream surface warpage, but should be applicable instead to highly rotational flows with large turning angles. The efficiency of the code developed for the solution of the secondary flows, has been demonstrated through comparisons with computing times of other existing methods [11]. The agreement between the results of the numerical computations of three dimensional rotational flow in a rectangular curved duct with existing experimental data has been demonstrated in the same reference.

EXPERIMENTAL WORK

The purpose of the experimental work is to obtain detailed accurate in-channel three-dimensional flow velocity measurements. The accuracy of the velocity measurements is very critical because of the flow field complexity. Additional problems in secondary flow measurements include the difference in the order of magnitude between the three velocity components and the possible ambiguity in defining the direction of the secondary velocities. The experimental measurements of this complex flow field are based on the use of a two-color, back scatter Laser Doppler Velocimeter system.

The Experimental Set-Up

The experimental set-up is shown schematically in Fig. 1. It consists of the tunnel, the particle feeder, the LDV System, the optical system, the data acquisition system, and the mechanical system for traversing the laser signal in the tunnel. The LDV and data acquisition systems have been acquired through an NSF equipment grant. The design of the experimental set-up is completed and the fabrication is near completion.

The LDV has been tested in another tunnel of simpler flow field using aluminum oxide powder as the seeding material, because of the relative ease of introducing it into the flow field. Through this experiment the accuracy of the velocity measurements have been tested and the data was found reproducible and precise enough to justify confidence in the experimental system. The various systems will be described and their design discussed in the following sections.

The Tunnel

The tunnel was designed to study the development of the distributed passage vortex, in order to use the results in evaluating the numerical code. For this purpose a constant area curved duct tunnel with a rectangular cross section was built to investigate the internal three dimensional rotational flow without the additional complexities of other turbomachinery effects such as stagnation point, tip clearance, trailing edge and spanwise pressure gradient. The tunnel is made of 3 mm thick plastic walls with screen vortex generator at inlet. The 90° turning angle curved duct whose cross section is 2 x 4 inches is constructed by cement welding two concentric cylindrical walls for the 5 inch and 7 inch duct inner and outer radii to the end walls. Cold bending is used in forming the cylindrical surfaces in order to avoid laser signal deformation.

The LDV and Optical Systems

A two color 4 watt laser system is used in backward scatter mode for the experimental measurements. The Spectra Physics Model 16409 argon-ion laser has blue and green beams of wave lengths 0.488 μ and 0.5145 μ, respectively. With the two color system, it is possible to measure two velocity components at right angles, simultaneously. Referring to Fig. 2, the beams go through the beam splitters, two 2" diameter mirrors and two 1" diameter mirrors. The blue beam is split into two beams in the horizontal plane and the green beam is split into two beams in the vertical plane. The polarity of the blue and green beams is adjusted through the polar rotators. A 4" diameter mirror is placed on the tunnel's axis of curvature, as shown in Fig. 3, to direct the beam at the desired position in the tunnel. For this purpose, the mirror is mounted on the rotational and radial control system. This system provides and controls the traverse motion of the mirror along the center axis of curvature of the tunnel as well as the mirror rotation around the optical axis. The rotational and radial control system is mounted on the optical systems table and a traverse motion along the table is allowed to change the distance between the big mirror and the receiving optics. The rotation of the 4" diameter mirror about the optical axis provides measurements along a constant radius arc. The traverse motion of the mirror along the center axis of curvature of the tunnel does not change the radius at which the measurements are obtained. A combination of these two motion surveys a cylindrical surface of constant radius. Through the lateral motion of the whole rotational and radial control system along the optics table to change its distance from this receiving optics, in addition to the mirror rotational and translational movements described previously, it will be possible to survey the whole flow field in the tunnel. Both the through flow (or circumferential) velocity component, and the lateral velocity component in the direction of the tunnel axis, will be performed with the mirror and the rotational and radial control system in place as shown in Figs. 1 and 2. In these measurements the LDV beams travel through the inner curved wall with the smaller radius of curvature. When measuring the radial velocity component, the mirror and the rotational and radial control system will be removed and the LDV system aligned so that the oncoming and reflected beams go through the non-curved side wall of the duct.

The Particle Feeder

A 9302 model atomizer is used for seeding the flow field with a 2.02 μ diameter polystyrene latex particle. The hydrosol of particles and water will be atomized such that each water droplet contains no more than one particle. A particle feeder will be constructed in our machine shop as shown in

Fig. 4 in the near future. According to the design, the atomizer output is mixed with dry air in a 1.8" ϕ tube before the water is condensed in a big chamber and the seeded air returned in a 3/8" ϕ tube.

The Data Acquisition System

Two TSI model 1990 signal processors are used to process the signals from the photo detectors. The signal processors are capable of handling frequencies ranging between 1 KHZ and 200 MHZ. The signal frequencies corresponding to the small secondary velocities fall into the pedestal noise frequency range where the noise levels are extremely high. The frequency shifter shifts the incoming signal frequency to the desired range where the noise levels are the lowest, and also resolves the ambiguity in the secondary flow velocity directions. A PDP 8/E computer is used to synchronize the data processors signals and to compute the velocity magnitude and direction. A computer program to provide histogram for both velocity magnitude and directions is written in assembler language.

Experimental Set-Up Design Calculations

While the measuring volume should be small for accuracy, the number of fringes in the measuring volume should be large enough to provide sufficient data points. Referring to Fig. 5, the following calculations were used in the design. The number of fringes, N_{FR}, in the measuring volume is inversely proportional to the fringe spacing, d_f, and can be determined from the following equation:

$$N_{FR} = \frac{d_m}{d_f}$$

where d_f is the fringe spacing and

$$d_m = 4\lambda f/\pi \; D_{e-2} \cos\kappa$$

where λ is the laser wave length, f is the focal length of the lense and, κ, is half the angle, ϕ, of the laser beam intersection as shown in Fig. 5. The fringe spacing is proportional to the wave length λ as given in the following equation:

$$d_f = \frac{\lambda}{2 \sin\kappa}$$

Referring to Fig. 5, the value of the different parameters in our system are as follows:

$d = 50$ mm

$\phi = 2\kappa = 11.05°$

$f = 250$ mm

and $D_{e-2} = 1.5$ mm

Using the above equations, the number of fringes in the measuring volume were calculated to be 44 for both green (λ = 4880°A) and blue (λ = 5145°A) beams. The expected frequency, F_D, at the photodetector can be determined from the following equation

$$F_D = \frac{2V \sin\kappa}{\lambda}$$

where V is the expected flow velocity.

Experimental Investigation of the Tunnel Wall Effect on the LDV Signal

The optical system design was proceeded by a systematic experimental study, to investigate the signal deterioration of the LDV system through the curved wall, which is critical to the accuracy of the flow velocity measurements. For this purpose, the green beam (λ = 514.5 mm argon multimode laser) was used in dual beam backward scatter mode through the 5 inch radius cylindrical plastic wall, as shown in Fig. 6. The signal was generated by fibers (ϕ = 0.005 in. ≃ 127 μm), attached on the perimeter of a rotating disk with a constant speed of 3400 rpm, measured by stroboflush-light. A memory scope was used to observe the burst signal. The cylindrical wall was positioned such that the axis of the optical system goes through the center of the radius of curvature. The experiments were conducted at different angles, namely 0°, 45° and 90°, between the plane of the dual beam and the axis of the dylindrical wall. The power level of the laser as well as the TSI data processor settings (filtering, min. cycles, expon., amplifier level) remained constant throughout all experiments. The investigation led to the following conclusions in regard to the effects of the wall curvature, thickness and initial stress due to bending on the LDV signal:

1. The polarization of the beams through the curved wall is not significantly deteriorated by the plastic material itself, nor by the initial stresses and the curvature.

2. The strength of the signal through the curved wall is reduced to approximately one-fourth of that without the wall.
3. The beams focusing point off-set by the wall thickness is not significant but that due to curvature is not.

ANALYTICAL WORK

The secondary flow in turbomachines resulting from the spanwise variation in the velocity of the flow entering the blade row is a complex three dimensional flow problem. Traditionally, turbomachinery flow fields are determined from two dimensional solutions which are obtained on two intersecting families of stream filaments with variable thickness. The governing equations are satisfied on the mean surfaces of these stream filaments, which are referred to as the S_1 (blade-to-blade) and the S_2 (meridional) surfaces. The correct solution of one family of surfaces requires some data from the other, and consequently, an iterative process between the solutions on these two families of surfaces is involved. Two techniques have been used to obtain solution on the S_1 or S_2 surfaces, namely the matrix method and the streamline curvature method.

In the streamline curvature method, the solution domain is covered with grid lines formed by the flow streamlines and orthogonals or quasi-orthogonals. The momentum equation is expressed in terms of the streamline's curvature to obtain velocity gradient equations. These equations are integrated along the orthogonals or the quasi-orthogonals for the flow velocities.

The continuity equation is then used to adjust the position of the streamlines. This process is repeated until the solution converges to a specified criteria.

In the matrix method, a stream function is defined to satisfy the continuity equation. When the velocity components are expressed in terms of the stream function and substituted in the equations of motion, a second order differential equation results, for the stream function. Iterative solutions, such as point and line successive over-relaxation methods, are commonly used for the solution of the stream function finite difference equations in turbomachinery flow computations.

Several problems are encountered in computing a synthesized three dimensional turbomachine flow field from the solutions on the S_1 and S_2 surfaces. These problems are related to the exchanged information between the two solutions such as the stream surfaces geometry and the stream filaments thickness. In the case of cascades with large turning angles, considerable stream surface twists, are caused by secondary flow. For this reason, the traditional quasi-three-dimensional flow solutions in turbomachines are not applicable to these highly rotational flow fields. Stuart and Hetherington [7] tried to study the rotational flow in a 90° bend by synthesizing a three-dimensional flow field through iterations between two dimensional solutions. They were unable to reach convergence in the iterative numerical solution and had to abandon this approach. They speculated that the information conveyed between the two solutions was not sufficient to produce convergence.

It is clear that the large stream surfaces warpage, the streamwise vorticity development, as well as the effects of both these phenomena on the through flow velocity, should be carefully modeled in any method that is developed for studying the three dimensional rotational flow in cascades. All these factors have been thoroughly investigated in developing the present analytical work. Throughout the formulation, the objective was also to develop a highly efficient numerical code, both in regard to computer time and storage requirements [11].

MATHEMATICAL FORMULATION

The primary dependent variables in the present analysis are the through flow velocity and vorticity components, and the streamlike function. The latter represents a new concept developed by Hamed and Abdallah [12], particularly for this study as a very effective method for the simultaneous numerical solution of the continuity and vorticity equations [13, 14]. The basic idea behind the mathematical formulation is to manipulate the governing equations in order to arrive at two first order hyperbolic equations in the through velocity and vorticity. The first of these is the component of Helmholtz equation in the through flow direction. The second is obtained through eliminating the total pressure from the momentum equations. These two equations are solved using a marching technique [15, 16] in the through flow direction. The streamlike function solution then provides the secondary velocity components.

The governing equations for rotational inviscid incompressible flow are first given in vector form as follows:

Continuity equation:

$$\nabla \cdot \bar{V} = 0 \tag{1}$$

Momentum equation:

$$\bar{V} \times \bar{\Omega} = \nabla P \tag{2}$$

where $\bar{V}$ is the velocity vector, P is the total pressure divided by the density, and $\bar{\Omega}$ is the vorticity vector which is defined as the curl of $\bar{V}$

$$\nabla \times \bar{V} = \bar{\Omega} \tag{3}$$

The formulation of the governing equations is based on the use of the vorticity component in the through flow direction as one of the dependent variables. For this purpose, it is more appropriate to replace one component of the momentum equation with a component of Helmholtz equation. This can be derived by taking the curl of the momentum equation (2) to give:

$$\nabla \times \bar{V} \times \bar{\Omega} = \nabla x \quad \nabla p \tag{4}$$

From vector identities,

$$\nabla \times \bar{V} \times \bar{\Omega} = \bar{\Omega} \cdot \nabla \bar{V} - \bar{\Omega}(\nabla \cdot \bar{V}) - (\bar{V} \cdot \nabla)\bar{\Omega} + \bar{V}(\nabla \cdot \bar{\Omega}) \tag{5}$$

$$\nabla \times \nabla p = 0 \tag{6}$$

and

$$\nabla \cdot \bar{\Omega} = 0 \tag{7}$$

Using equations (1), (5), (6) and (7) into equation (4), we obtain Helmholtz equation which is used in the analysis

$$\bar{V}\cdot\nabla\bar{\Omega} = \bar{\Omega}\cdot\nabla\bar{V} \tag{8}$$

The cylindrical coordinate system is used in the analysis to simplify the boundary conditions in the constant area duct of Fig. 7. Equations (1), (2) and (8) are rewritten in these coordinates as follows:

Continuity equation:

$$\frac{\partial u}{\partial r} + \frac{u}{r} + \frac{1}{r}\frac{\partial v}{\partial \theta} + \frac{\partial w}{\partial z} = 0 \tag{9}$$

Momentum equation:

r-component,

$$v\zeta - w\xi = \frac{\partial P}{\partial r} \tag{10}$$

θ-component,

$$w\eta - u\zeta = \frac{1}{r}\frac{\partial P}{\partial \theta} \tag{11}$$

z-component,

$$u\xi - v\eta = \frac{\partial P}{\partial z} \tag{12}$$

where u, v and w are the r, θ and z components of velocity and η, ξ and ζ are the r, θ and z components of vorticity defined as follows,

$$\eta = \frac{1}{r}\frac{\partial w}{\partial \theta} - \frac{\partial v}{\partial z} \tag{13a}$$

$$\xi = \frac{\partial u}{\partial z} - \frac{\partial w}{\partial r} \tag{13b}$$

$$\zeta = \frac{\partial v}{\partial r} + \frac{v}{r} - \frac{1}{r}\frac{\partial u}{\partial \theta} \tag{13c}$$

Helmholtz equation:

r-component,

$$u\frac{\partial \eta}{\partial r} + \frac{v}{r}\frac{\partial \eta}{\partial \theta} + w\frac{\partial \eta}{\partial z} = \eta\frac{\partial u}{\partial r} + \frac{\xi}{r}\frac{\partial u}{\partial \theta} + \zeta\frac{\partial u}{\partial z} + \frac{1}{r}(u\xi - v\eta) \tag{14}$$

θ-component,

$$u\frac{\partial \xi}{\partial r} + \frac{v}{r}\frac{\partial \xi}{\partial \theta} + w\frac{\partial \xi}{\partial z} = \eta\frac{\partial u}{\partial r} + \frac{\xi}{r}\frac{\partial v}{\partial \theta} + \zeta\frac{\partial v}{\partial z} - \frac{1}{r}\left(u\xi - \frac{v}{r}\eta\right) \tag{15}$$

z-component,

$$u\frac{\partial \zeta}{\partial r} + \frac{v}{r}\frac{\partial \zeta}{\partial \theta} + w\frac{\partial \zeta}{\partial z} = \frac{\partial w}{\partial r} + \frac{\xi}{r}\frac{\partial w}{\partial \theta} + \zeta\frac{\partial w}{\partial z} \tag{16}$$

Initial and Boundary Conditions:

Referring to Fig. 7, the following initial and boundary conditions are used.

$$v(r,0,z) = v_I(r,z) \tag{17a}$$

$$\zeta(r,0,z) = 0 \tag{17b}$$

$$u(R_i,\theta_1,z) = u(R_0,\theta_2,z) = 0 \tag{18a}$$

$$w(r,\theta,0) = w(r,\theta,H) = 0 \tag{18b}$$

The through flow vorticity component, ξ, is determined from the solution of equation (15). The other two components of Helmholtz equations (14), (16), and the momentum equations (10) to (12) are manipulated to arrive at the differential equation which is solved for the through flow velocity component v. The cross velocity components u and w are calculated from the simultaneous solution of the continuity equation (9) and the vorticity equation (13b) at constant θ.

Derivation of the Through Flow Velocity Equation

Using the total derivative operator with equations (10) and (12), we obtain:

$$v\cdot\nabla(u\xi - v\eta) = \vec{v}\cdot\nabla\left(\frac{\partial P}{\partial z}\right) \tag{19a}$$

$$\vec{v}\cdot\nabla(v\zeta - w\xi) = \vec{v}\cdot\nabla\left(\frac{\partial P}{\partial r}\right) \tag{19b}$$

Equations (19a) and (19b) can be expanded and rearranged in the following form

$$\eta(\vec{v}\cdot\nabla v) = \xi(\vec{v}\cdot\nabla u) + u(\vec{v}\cdot\nabla\xi) - v(\vec{v}\cdot\nabla\eta) - \vec{v}\cdot\nabla\ \left(\frac{\partial P}{\partial z}\right) \tag{20a}$$

and

$$\zeta(\vec{v}\cdot\nabla v) = \vec{v}\cdot\nabla\left(\frac{\partial P}{\partial r}\right) - v(\vec{v}\cdot\nabla\xi) + \xi(\vec{v}\cdot\nabla w) + w(\vec{v}\cdot\nabla\xi) \tag{20b}$$

The term $\vec{v}\cdot\nabla\left(\frac{\partial P}{\partial z}\right)$ in equation (20a) can be expressed in terms of the velocity components u, v, w and the through flow vorticity ξ as follows:

$$\vec{v}\cdot\nabla\left(\frac{\partial P}{\partial z}\right) = \frac{\partial}{\partial z}\ (\vec{v}\cdot\nabla p) - \frac{\partial \vec{v}}{\partial z}\cdot\nabla p \tag{21}$$

On using the momentum equations (10), (11) and (12) in equation (21) one obtains:

$$
\begin{aligned}
\bar{V}\cdot\nabla\left(\frac{\partial P}{\partial z}\right) = &- \frac{\partial u}{\partial z}\left[v\left(\frac{\partial v}{\partial r} + \frac{v}{r} - \frac{1}{r}\frac{\partial u}{\partial \theta}\right) - w\xi\right] \\
&- \frac{\partial v}{\partial z}\left[w\left(\frac{1}{r}\frac{\partial w}{\partial \theta} - \frac{\partial v}{\partial z}\right) - u\left(\frac{\partial v}{\partial r} + \frac{v}{r} - \frac{1}{r}\frac{\partial u}{\partial \theta}\right)\right] \\
&- \frac{\partial w}{\partial z}\left[u\xi - v\left(\frac{1}{r}\frac{\partial w}{\partial \theta} - \frac{\partial v}{\partial z}\right)\right]
\end{aligned}
\tag{22a}
$$

Similarly, using the momentum equation, equation (20b) can be written as follows

$$
\begin{aligned}
\bar{V}\cdot\nabla\left(\frac{\partial P}{\partial r}\right) = &- \frac{\partial u}{\partial r}\left[v\left(\frac{\partial v}{\partial r} + \frac{v}{r} - \frac{1}{r}\frac{\partial u}{\partial \theta}\right) - w\xi\right] \\
&+ \left(\frac{v}{r} - \frac{\partial v}{\partial r}\right)\left[w\left(\frac{1}{r}\frac{\partial w}{\partial \theta} - \frac{\partial v}{\partial z}\right) - u\left(\frac{\partial v}{\partial r} + \frac{v}{r} - \frac{1}{r}\frac{\partial u}{\partial \theta}\right)\right] \\
&- \frac{\partial w}{\partial r}\left[u\xi - v\left(\frac{1}{r}\frac{\partial w}{\partial \theta} - \frac{\partial v}{\partial z}\right)\right]
\end{aligned}
\tag{22b}
$$

Expanding equations (20a) and (20b) in full and using equations (22a) and (22b), we obtain:

$$
\begin{aligned}
u\frac{\partial v}{\partial r} + \frac{v}{r}\frac{\partial v}{\partial \theta} + w\frac{\partial v}{\partial z} = &\left\{w\left(u\frac{\partial \xi}{\partial r} + \frac{v}{r}\frac{\partial \xi}{\partial \theta} + w\frac{\partial \xi}{\partial z}\right) + \xi w\frac{\partial w}{\partial z}\right. \\
&- v\left(\frac{\partial v}{\partial r} + \frac{v}{r} - \frac{1}{r}\frac{\partial u}{\partial \theta}\right)\frac{\partial w}{\partial z} - \frac{\partial u}{\partial r}\left[v\left(\frac{\partial v}{\partial r} + \frac{v}{r} - \frac{1}{r}\frac{\partial u}{\partial \theta}\right) - w\xi\right] \\
&\left.- \left(\frac{\partial v}{\partial r} - \frac{v}{r}\right)\left[w\left(\frac{1}{r}\frac{\partial w}{\partial \theta} - \frac{\partial v}{\partial z}\right) - u\left(\frac{\partial v}{\partial r} + \frac{v}{r} - \frac{1}{r}\frac{\partial u}{\partial \theta}\right)\right]\right\}/ \\
&\left(\frac{\partial v}{\partial r} + \frac{v}{r} - \frac{1}{r}\frac{\partial u}{\partial \theta}\right)
\end{aligned}
\tag{23a}
$$

and

$$
\begin{aligned}
u \frac{\partial v}{\partial r} + \frac{v}{r} \frac{\partial v}{\partial \theta} + w \frac{\partial v}{\partial z} = \{ & u(u \frac{\partial \xi}{\partial r} + \frac{v}{r} \frac{\partial \xi}{\partial \theta} + w \frac{\partial \xi}{\partial z}) + \xi u \frac{\partial u}{\partial r} \\
& - v(\frac{1}{r} \frac{\partial w}{\partial \theta} - \frac{\partial v}{\partial z}) \frac{\partial u}{\partial r} - \frac{\partial w}{\partial z} [v(\frac{1}{r} \frac{\partial w}{\partial \theta} - \frac{\partial v}{\partial z}) - u\xi] + \frac{\partial v}{\partial z} [w(\frac{1}{r} \frac{\partial w}{\partial \theta} - \frac{\partial v}{\partial z}) \\
& - u(\frac{\partial v}{\partial r} + \frac{v}{r} - \frac{1}{r} \frac{\partial u}{\partial \theta})]\}/(\frac{1}{r} \frac{\partial w}{\partial \theta} - \frac{\partial v}{\partial z}) \qquad (23b)
\end{aligned}
$$

Derivation of the Streamlike Function Equation

Equations (9) and (13b) are two coupled first order equations in u and w. Their simultaneous solution succeeds the through flow velocity and vorticity computations from equations (15) and (23). Equations (9) and (13b) are first rewritten as follows:

$$\frac{\partial u}{\partial r} + \frac{u}{r} + \frac{\partial w}{\partial z} = - \frac{1}{r} \frac{\partial v}{\partial \theta} \qquad (24)$$

$$\frac{\partial u}{\partial z} - \frac{\partial w}{\partial r} = \xi \qquad (25)$$

In this form, it is clear that the source/sink term in the right hand side of equation (24) is caused by the variation of the through flow velocity, v, in the θ direction.

The simultaneous solution of equations (24) and (25) is obtained using the streamlike function formulation [12, 13]. Through this formulation, the two coupled first order equations (24) and (25) are transformed into a single second order equation with Dirichlet boundary conditions.

Hamed and Abdallah [12, 13] defined a streamlike function, χ, which identically satisfies the continuity equation with the source term. According to this definition, the cross velocity components u and w are related to χ through the following expressions

$$u = \frac{1}{r}\frac{\partial \chi}{\partial z} + \frac{1}{r}\int_{R_i}^{r} \left(-\frac{\partial v}{\partial \theta}\right) dr \tag{26}$$

and

$$w = -\frac{1}{r}\frac{\partial \chi}{\partial r} \tag{27}$$

The deviation from the standard definition of the stream function formulation is in the extra integral term of equation (28), for the velocity component u.

When equations (26) and (27) are substituted into equation (25), one obtains:

$$\frac{\partial^2 \chi}{\partial r^2} - \frac{1}{r}\frac{\partial \chi}{\partial r} + \frac{\partial^2 \chi}{\partial z^2} = r\xi + \frac{\partial}{\partial z}\int_{R_i}^{r} \frac{\partial v}{\partial \theta}\, dr \tag{28}$$

Equation (28) is solved for the streamlike function χ using successive over relaxation, then equations (26) and (27) are used to calculate the two velocity components u and w. The following boundary conditions for the streamlike function, χ, are obtained by substituting equations (26) and (27) into equations (18a) and (18b).

$$\frac{\partial \chi}{\partial z} = \int_{R_i}^{R_o} \frac{\partial v}{\partial \theta}\, dr \qquad \text{at } r = R_i \text{ and } r = R_o \tag{29}$$

$$\frac{\partial \chi}{\partial \theta} = 0 \qquad \text{at } z = 0 \text{ and } z = H \tag{30}$$

Integrating the derivatives on the right hand side of equations (29) and (30) along the duct cross section boundaries, yields Dirichlet boundary conditions for the streamlike function χ.

RESULTS

The numerical solution of the governing equations is obtained in a 90° turning duct with rectangular cross-section. The experimental data of reference [17], which is obtained for a flow field with substantial inlet velocity variation, is used in the assessment of the present analysis. The same data was used for comparison with the numerical results in references [7] and [8]. The flow measurements were reported at the 30°, 60° and 90° turning angles of a rectangular duct, with a 15" mean radius and a 5 x 10 inch cross-section. The duct geometry and dimensions are shown in Fig. 7. The experimentally measured inlet profile of reference [17] is reproduced in Fig. 8. It can be seen from this figure that the variations in the profile are greater in the low velocity regions compared to the nearly uniform velocity at the center line. In addition it may be observed that the variation in the radial direction is not too significant. The inlet velocity used in the numerical solution had a parabolic profile in the z-direction. Due to the symmetry of the inlet profile the computations are carried out only in the lower half of the duct. The governing equations were non-dimensionalized before the numerical solution, so that all the results, except the velocity contours, are presented in the non-dimensional form. The duct inner radius, R_i, and the maximum flow velocity at inlet, $V_{I_{max}}$, were used in the normalization.

The results are presented in the form of secondary vorticity and through flow velocity contours, and vectors showing the magnitude and direction of the secondary velocities. Figures 9, 10 and 11 present the results of the computations at 30°, 60° and 90° turning angles, respectively. Due to the symmetry of the inlet profile, the results are presented in the lower duct half. It can be seen from these figures (9a, 10a and 11a) that the vortex center is generally closer to the end wall. Because of the symmetry of the inlet profile, the generated secondary vorticity is assymmetric. It would be negative in the upper duct half, and vanishes at the plane of symmetry. The center of secondary vorticity can be seen to move towards the outer curved wall between 30° and 90° turning angles. A comparison of Figures 9a, 10a and 11a reveals that the generated secondary vorticity reaches a maximum at the 30° cross-section, then decreases at higher turning angles. Figure 11a shows a larger region of low secondary vorticity near the plane of symmetry at the 90° cross-section. This region also extends to the inner corner where negative vorticity starts to develop. The corresponding variations in secondary velocities can be seen in Figs. 9b, 10b and 11b. It can be seen from these figures that, while the secondary velocities are comparable in magnitude at the 30° and 60° duct cross-sections, they are significantly smaller at the 90° cross-section. The secondary velocities are particularly very small near the plane of symmetry at the 90° section, which is the region of very small secondary vorticity. The center of rotation in Figs. 9b, 10b and 11b is different from the vortex center in Figs. 9a, 10a and 11a. This difference can be attributed to the source term in the continuity equation which is caused by the variation in the through flow velocity component in θ-direction. It can be noticed from these figures, that between 30° and 90° cross-sections, the center of rotation has moved outwards and upwards.

The velocity contours are shown in Figs. 9c, 10c and 11c for 30°, 60° and 90° turning angles. Significant rotation of the through velocity contours can be observed in the first 60° of the duct, from their original parallel horizontal shape. The contours become nearly vertical before their rotation rate starts to decrease for turning angles greater than 60°. In particular, no significant rotation of the velocity contours can be observed near the axis of symmetry at the 90° turning angle.

DISCUSSION AND CONCLUSIONS

The results of the present analysis were compared to the experimental data of reference [17]. The same flow field was investigated in references [7], [8] and [18]. The first two of these references represent inviscid flow solutions, while the last represents a viscous flow solution. The present analysis was compared to these investigations [11], in terms of agreement with the experimental data of reference [17] and also in terms of the computer time requirements. It was concluded from that comparison that the present analysis prediction of the rotation of the constant velocity contours, as well as the velocity magnitudes, is generally satisfactory. The agreement between the present analysis and the experimental data is very significant in the high velocity regions, where the viscous effects are not dominant. The viscous solution [18] fails to predict the rotation of the high velocity contours, as well as the magnitude of the velocity in this region [11]. The inviscid solution of reference [7], on the other hand, gives satisfactory results in the high velocity regions but is in poor agreement with the experimental data in the low velocity regions.

In the present study, numerical computations were carried out in double precision on AMDAHL 470 V/6-II. Using a (11 x 11 x 45) grid, the computer time was 20 seconds. Fagan [8], using the total of six stream surfaces, with 200 nodal points per surface reported a CPU time of 1500-2100 seconds on the IBM 370/155. Stuart and Hetherington [7], reported a CPU time of 840 seconds on the IBM 360/65; using a (9 x 8 x 15) grid. Roscoe [18] used an (8 x 8 x 16) grid to obtain his solution, and reported a CPU time of 550 seconds on CDC 7600. It can be concluded therefore that the basic secondary flow phenomenon is well represented by the present analysis. In addition, the computer time in the present study is significantly smaller than the computer time in references [7], [8] and [18].

REFERENCES

1. Salvage, J., "Investigation of Secondary Flow Behavior and End Wall Boundary Layer Development Through Compressor Cascades," VKI TN 107, 1974.

2. Woods, J.R., "An Investigation of Secondary Flow Phenomena and Associated Losses in a High Deflection Turbine Cascade," Naval Postgraduate School, Monterey, California, NTIS Report No. AD750-183, 1972.

3. Lakshminarayana, B. and Horlock, J., "Leakage and Secondary Flow in Compressor Cascades," ARC R&M No. 3483, 1967.

4. Squire, H.B. and Winter, K.G., "The Secondary Flow in a Cascade of Aerofoils in a Non-Uniform Stream," Journal of Aeronautical Sciences, Vol. 18, 1951, p. 271.

5. Hawthorne, W.R., "Some Formulae for the Calculation of Secondary Flow in Cascades," ARC Report 17519, 1955.

6. Wu, C.H., "A General Theory of Three Dimensional Flow in Subsonic Turbomachines of Axial, Radial and Mixed Flow Types," NACA TN 2604, 1952.

7. Stuart, A.R. and Hetherington, R., "The Solution of the Three Variable Duct Flow Equations," NASA SP 304, Fluid Mechanics, Acoustics and Design of Turbomachines, Part I, 1974, pp. 135-150.

8. Fagan, J.R., "Three-Dimensional Subsonic Duct Flow Analysis," Detroit Diesel Allison, Div. of General Motors Corp., EDR7451, 1972.

9. Horlock, J., "Recent Developments in Secondary Flow," Paper No. 1, AGARD Conference Proceedings No. 214, on Secondary Flow in Turbomachines, March 1977.

10. Hamed, A., "Three Dimensional Internal Flow in Turbomachinery-Task 1: Secondary Flow in Diffusing Cascade," Annual Technical Report, December 1979.

11. Abdallah, S. and Hamed, A., "An Inviscid Solution for the Secondary Flow in Curved Ducts," AIAA Paper 80-1116, 1980.

12. Hamed, A. and Abdallah, S., "Streamlike Function: A New Concept in Flow Problems Formulation," Journal of Aircraft, Vol. 16, No. 12, December 1979, p. 801.

13. Hamed, A. and Abdallah, S., "A New Approach for Solving the Vorticity and Continuity Equations in Turbomachinery Ducts," AIAA Paper No. 79-0046, January 1979.

14. Hamed, A. and Abdallah, S., "Three Dimensional Rotational Flow in Highly Curved Ducts Due to Inlet Vorticity," AIAA Paper 78-146, 1978.

15. Lax, P.D. and Wendroff, B., "Systems of Conservation Laws," Communications on Pure and Applied Mathematics, Vol. 13, pp. 217-237, 1960.

16. Lax, P.D. and Wendroff, B., "Difference Schemes with High Order of Accuracy for Solving Hyperbolic Equations," Communications on Pure and Applied Mathematics, Vol. 17, p. 381, 1969.

17. Joy, W., "Experimental Investigation of Shear Flow in Rectangular Bends," M.S. Thesis, Massachusetts Institute of Technology, 1950.

18. Roscoe, D.F., "The Numerical Solution of the Navier-Stokes Equations for a Three-Dimensional Laminar Flow in Curved Pipes Using Finite Difference Methods," Journal of Engineering Mathematics, Vol. 12, No. 4, October 1978, pp. 303-323.

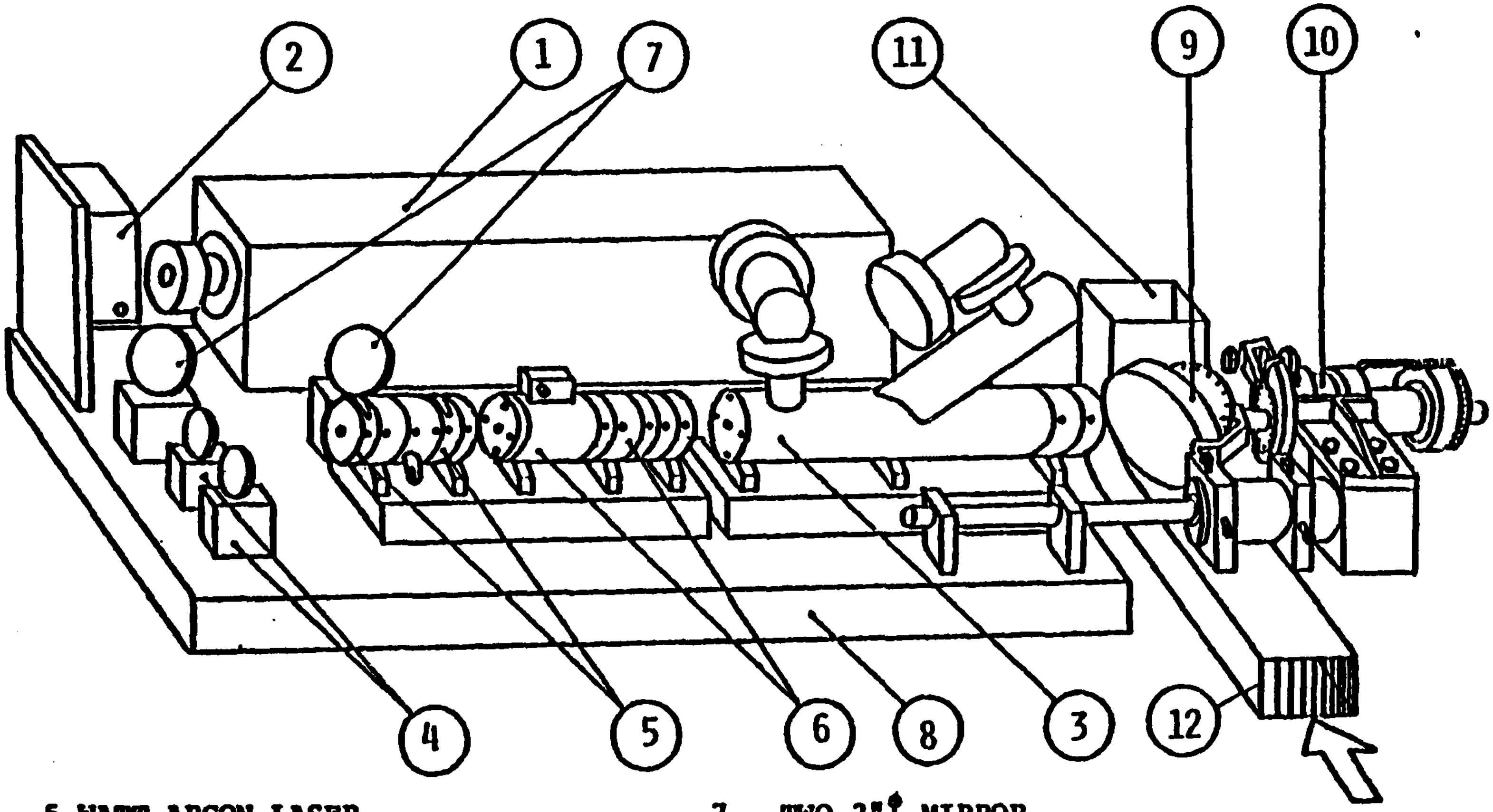

1. 5 WATT ARGON LASER
2. BEAM SLPITTER
3. RECEIVING OPTICS & PHOTODETECTORS
4. TWO 1"Φ MIRROR
5. BEAM SPLITTER & POLAR ROTATOR
6. FREQUENCY SHIFTERS
7. TWO 2"Φ MIRROR
8. THE OPTICAL SYSTEM'S TABLE
9. 4"Φ MIRROR
10. THE ROTATIONAL & RADIAL CONTROL SYSTEM
11. THE 90° RECTANGULAR BEND
12. VORTEX GENERATOR

FIG. 1. SCHEMATIC DRAWING OF THE EXPERIMENTAL SET-UP TO MEASURE THE ROTATIONAL FLOW IN A RECTANGULAR BEND.

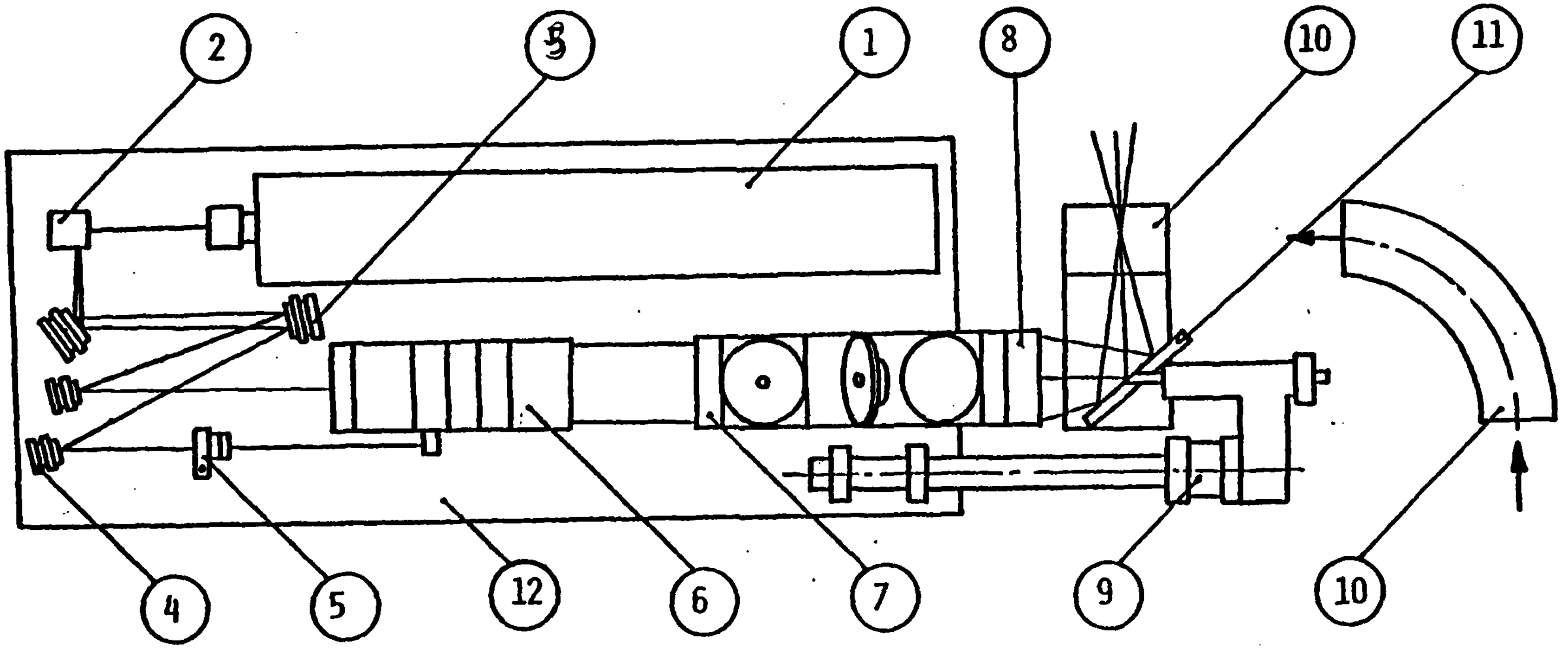

1. 5 WATT ARGON LASER
2. BEAMSPLITTER
3. TWO 2" DIAMETER MIRRORS
4. TWO 1" DIAMETER MIRRORS
5. POLARIZATION ROTATOR
6. BEAMSPLITTER & POLARIZATION ROTATOR.
7. BACKSCATTER RECEIVING OPTICS WITH COLOR SPLITTER
8. 250 MM LENS
9. ROTATIONA AND RADIAL CONTROL SYSTEM
10. RECTANGULAR BEND 4" x 2"
11. 4" DIAMETER MIRROR
12. THE OPTICAL SYSTEM TABLE.

FIG. 2. SCHEMATIC DRAWING OF LDV AND OPTICAL CONFIGURATION.

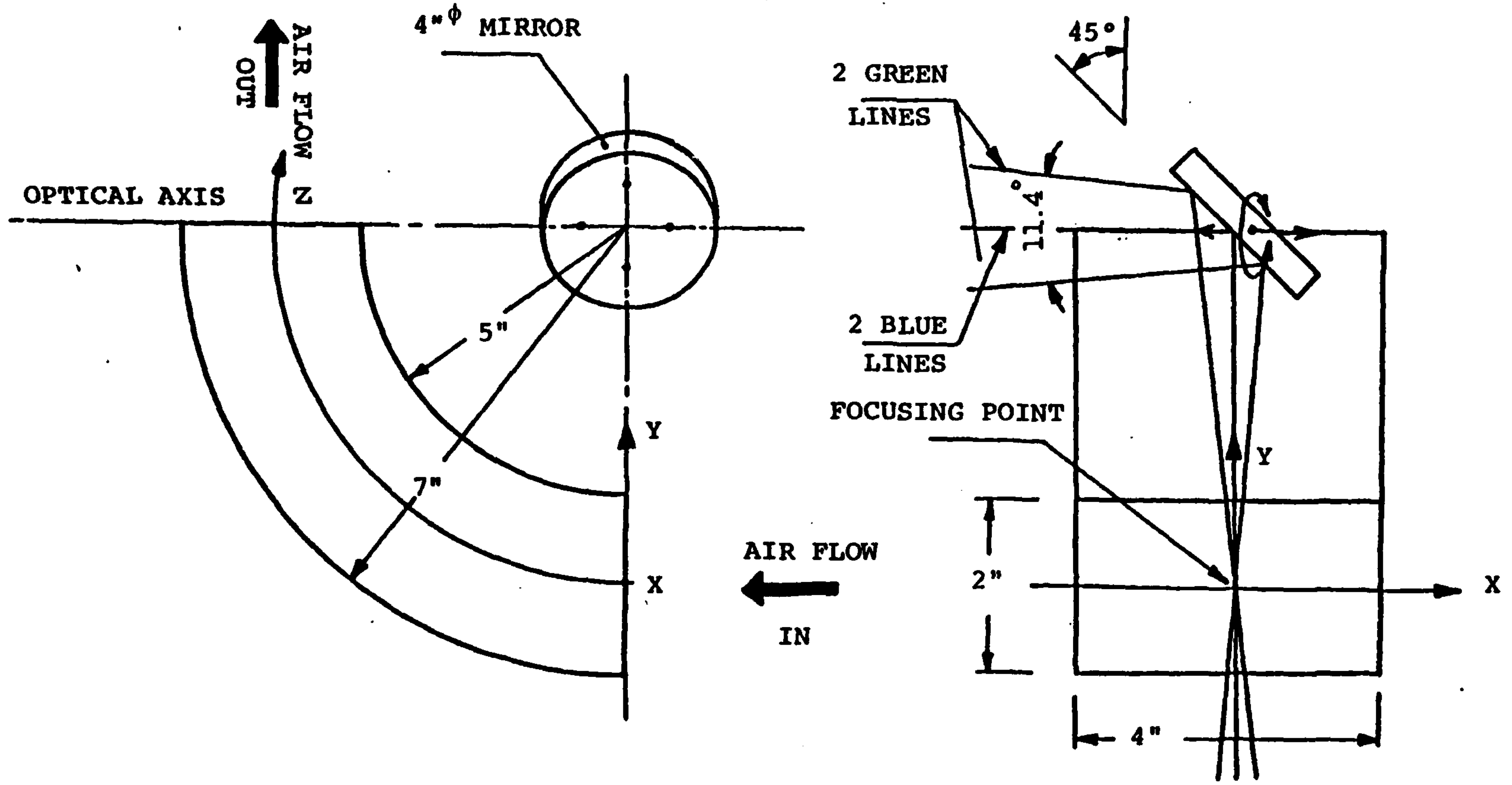

FIG. 3. THE MIRROR POSITION RELATIVE THE RECTANGULAR BEND WITH ITS DEGREES OF FREEDOM.

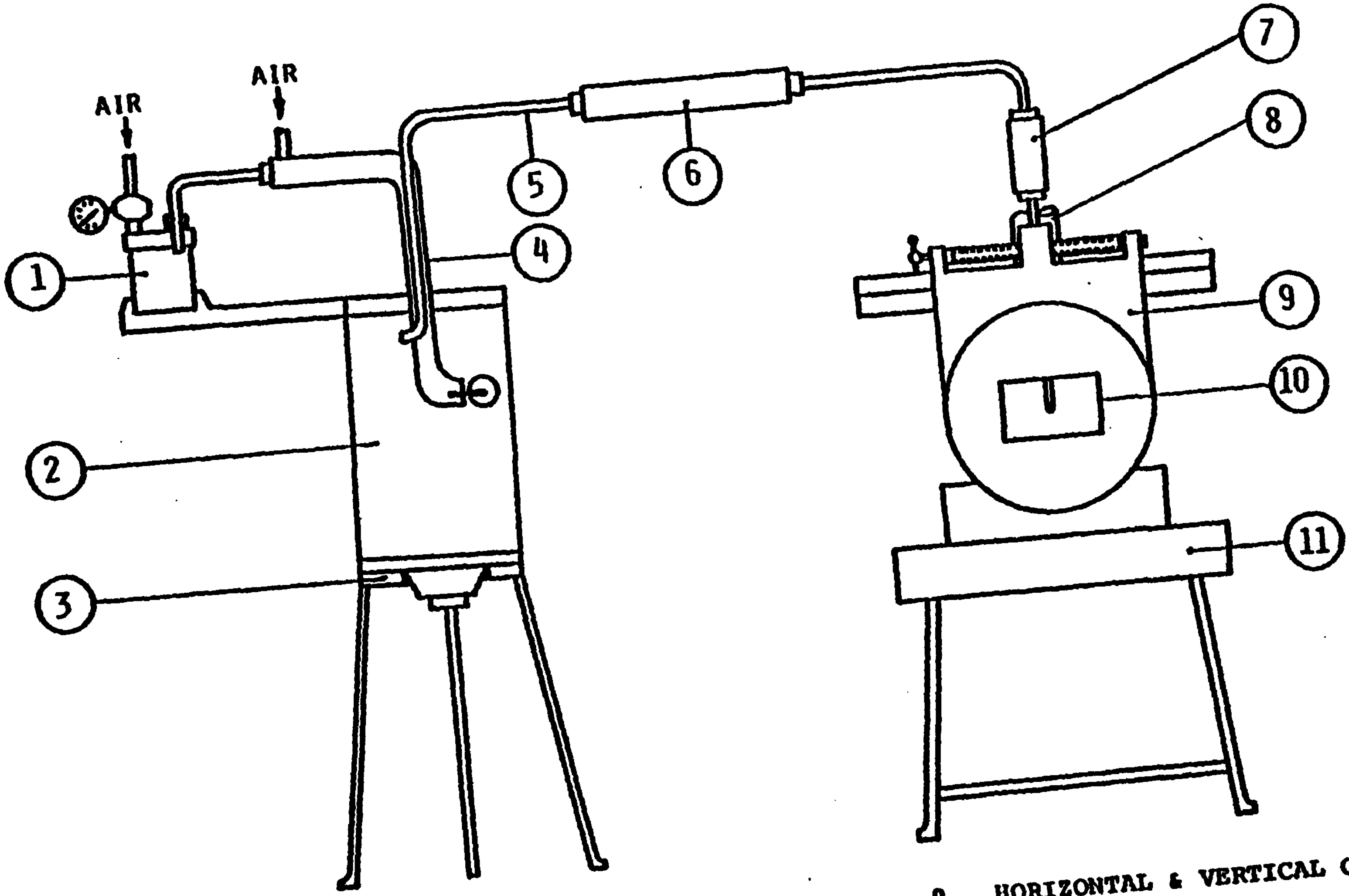

1. MODEL 9302 ATOMIZER
2. AIR DRAINER
3. AIR DRAINER CARRIER
4. 1.8"ϕ TUBE
5. 3/8"ϕ TUBE
6. HORIZONTAL TRAVELING TUBE
7. VERTICAL TRAVELING TUBE
8. THE MAIN AIR ENTRANCE
9. HORIZONTAL & VERTICAL CONTROL SYSTEM.
10. THE TEST SECTION
11. WIND TUNNEL TABLE

FIG. 4. SCHEMATIC DRAWING OF THE PARTICLE FEEDER AND TEST SECTION.

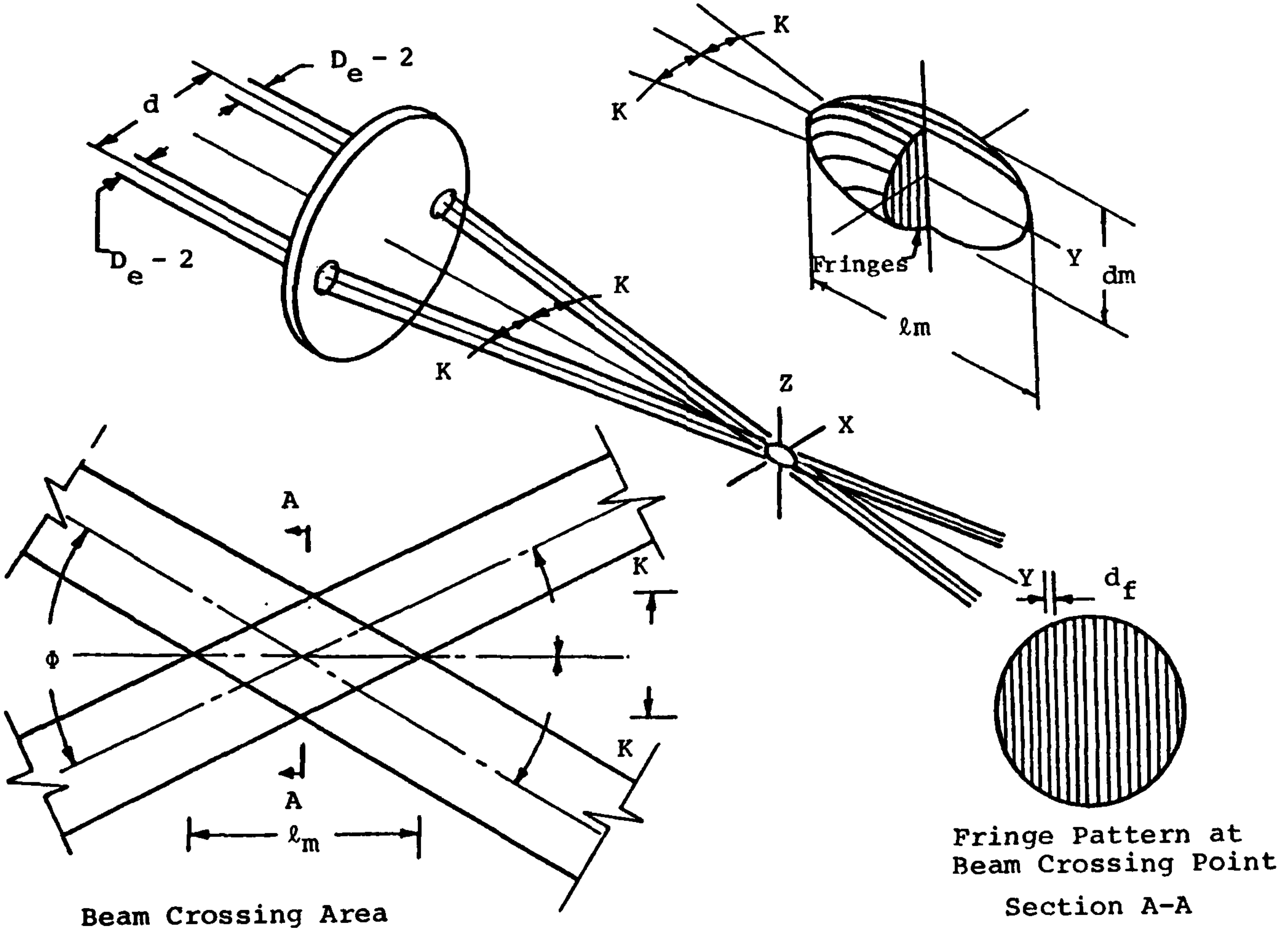

Beam Crossing Area

Fringe Pattern at
Beam Crossing Point

Section A-A

FIG. 5. THE MEASURING VOLUME.

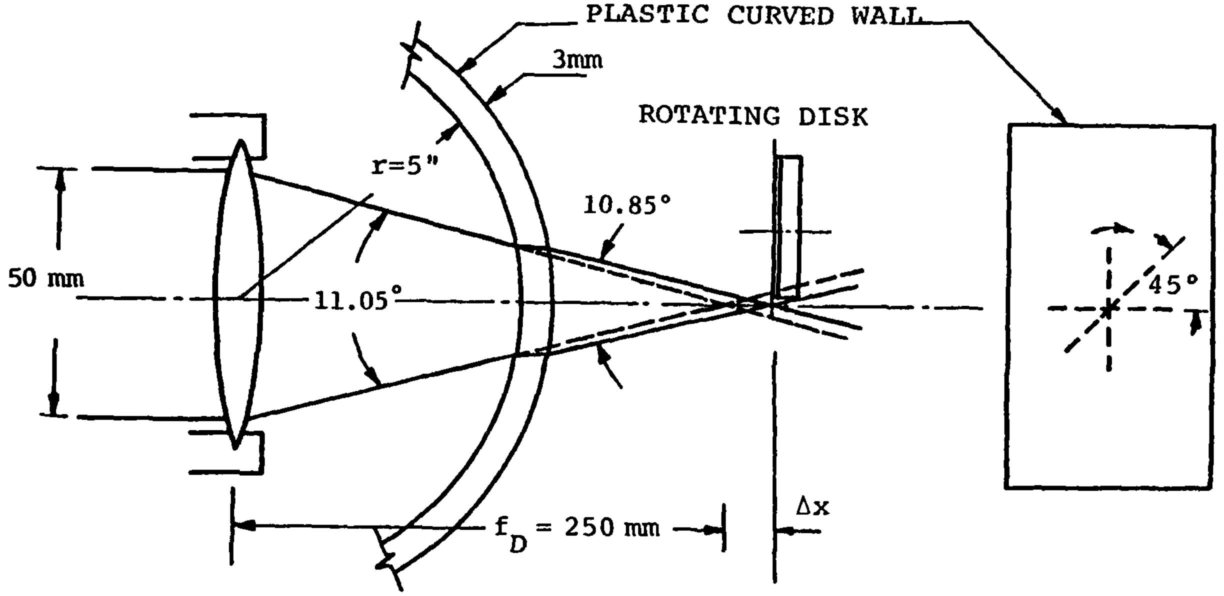

FIG. 6. THE EFFECT OF THE PLASTIC CURVED WALL ON THE FOCUSING POINT.

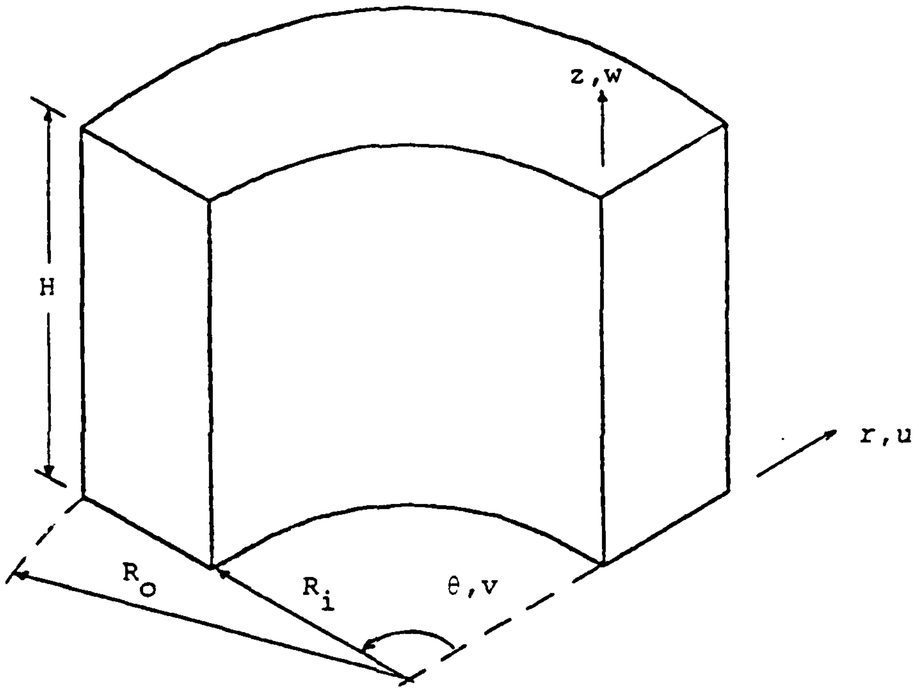

R_i = 12.5"

R_o = 17.5"

H = 10"

FIG. 7. DUCT GEOMETRY.

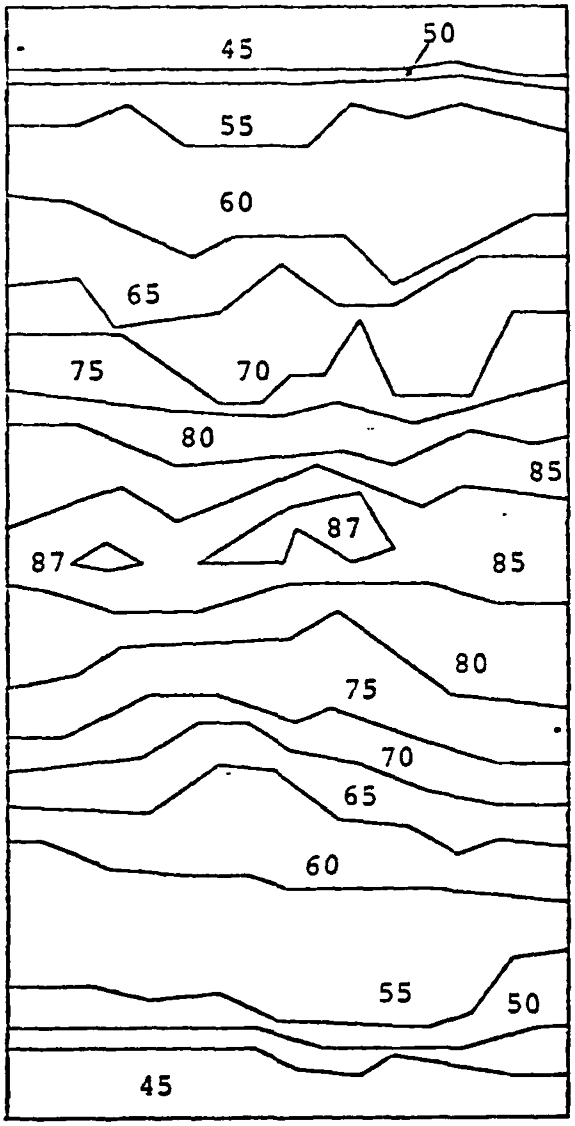

FIG. 8. INLET VELOCITY CONTOURS,
EXPERIMENTAL DATA, REF. (17).

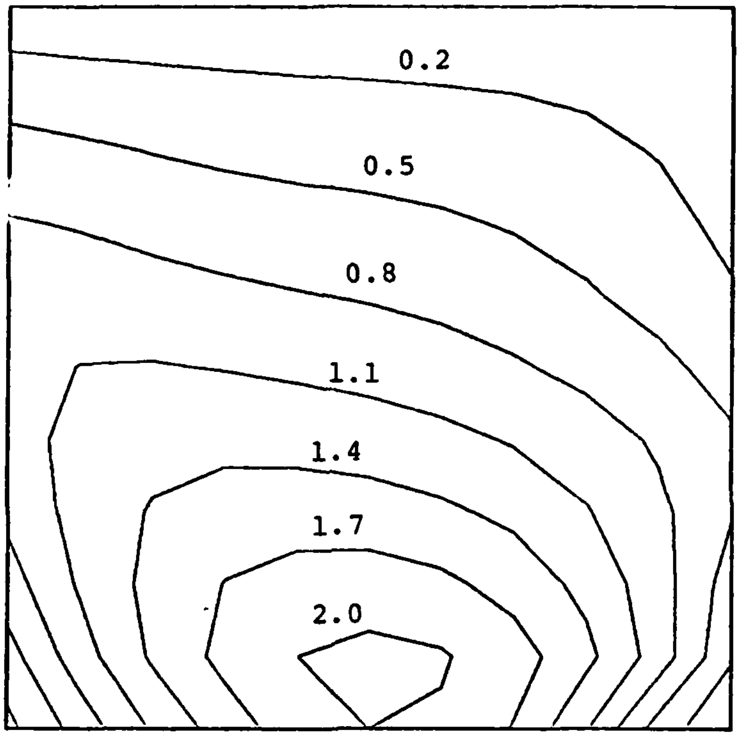

FIG. 9A. SECONDARY VORTICITY, θ = 30°.

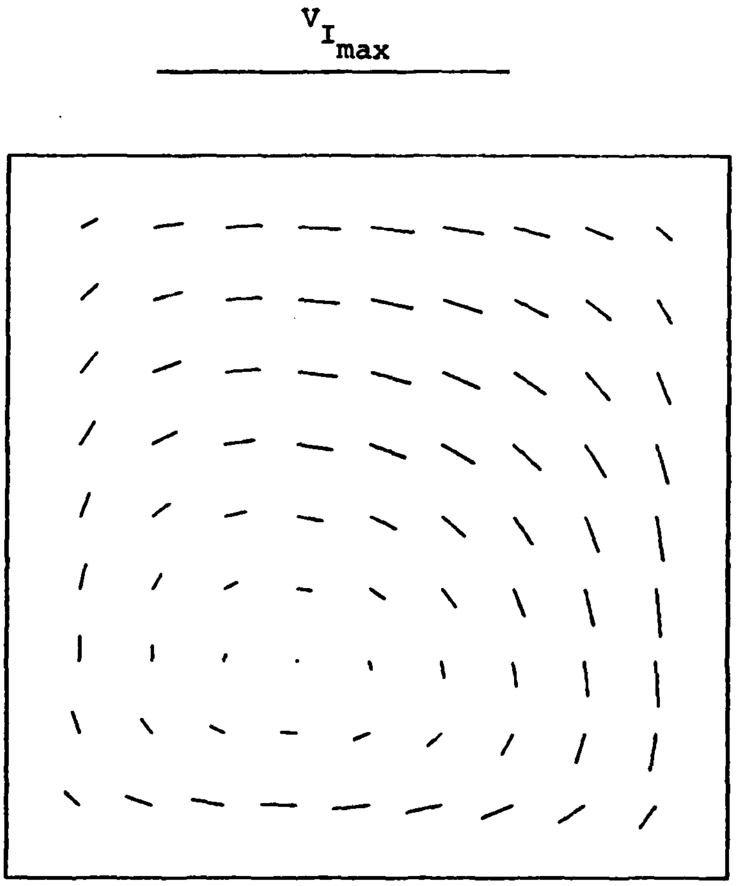

FIG. 9B. SECONDARY VELOCITIES, θ = 30°.

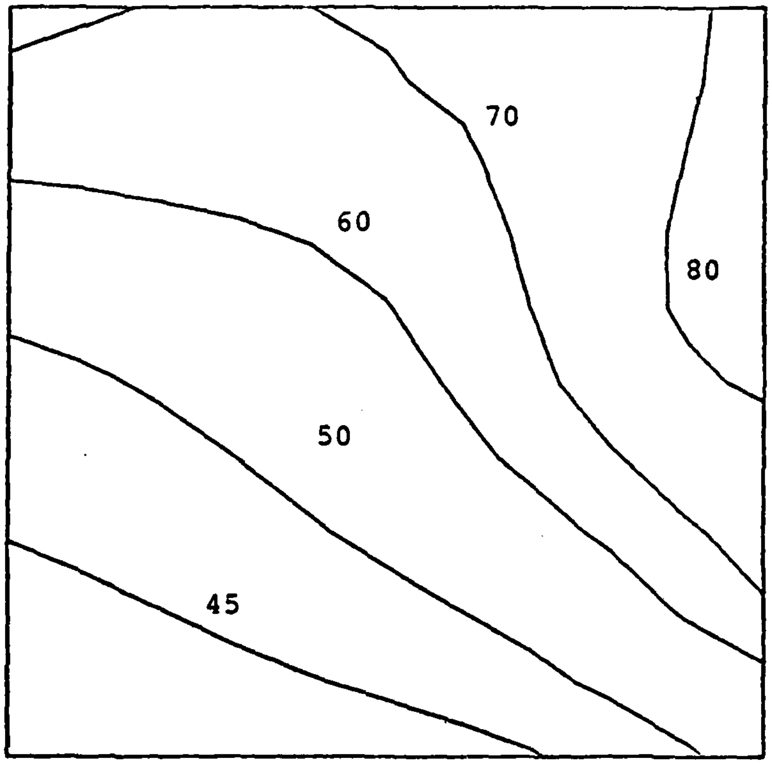

FIG. 9c. VELOCITY CONTOURS AT θ = 30°.

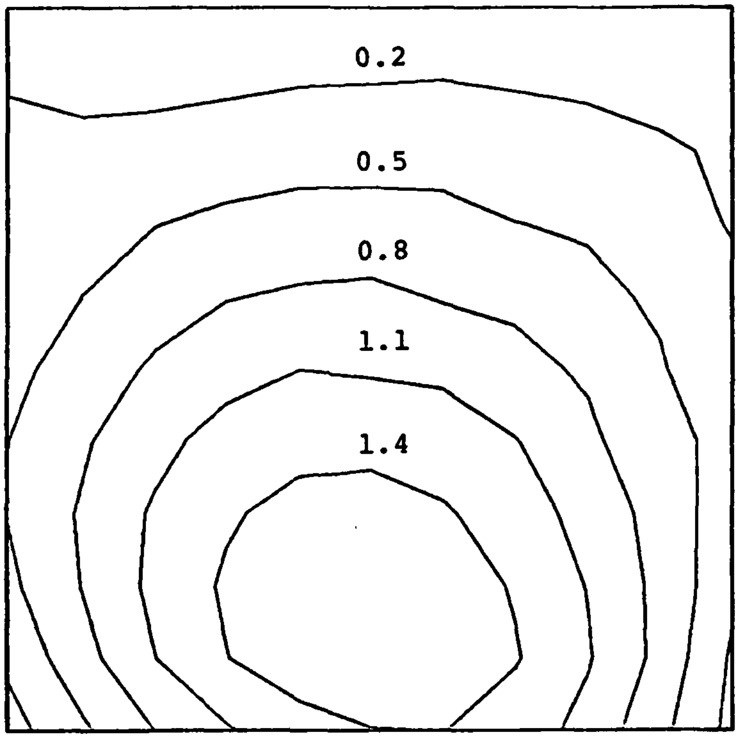

FIG. 10A. SECONDARY VORTICITY, $\theta = 60°$..

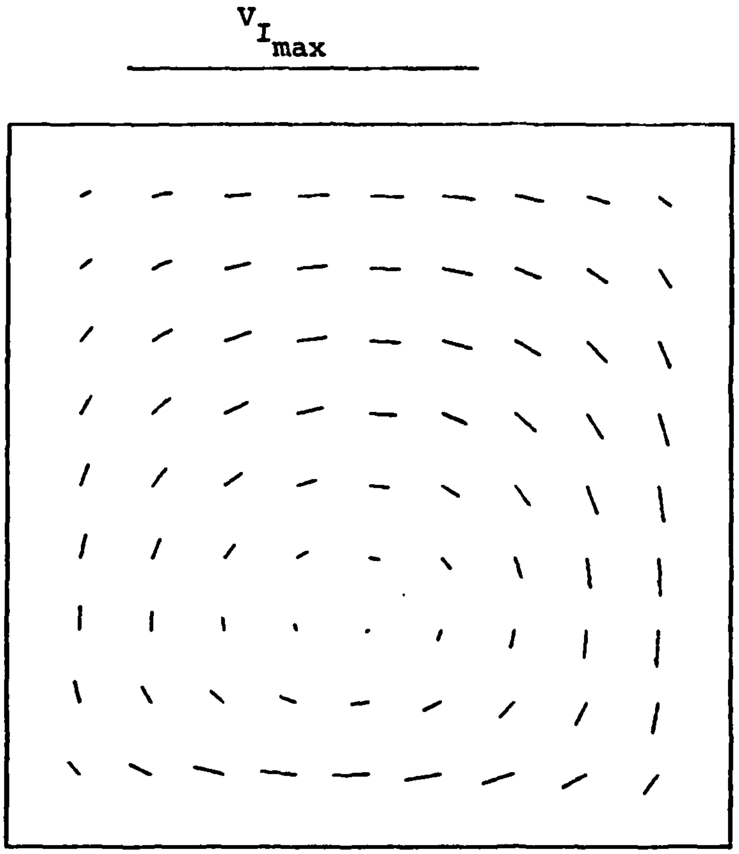

FIG. 10B. SECONDARY VELOCITIES, θ = 60°.

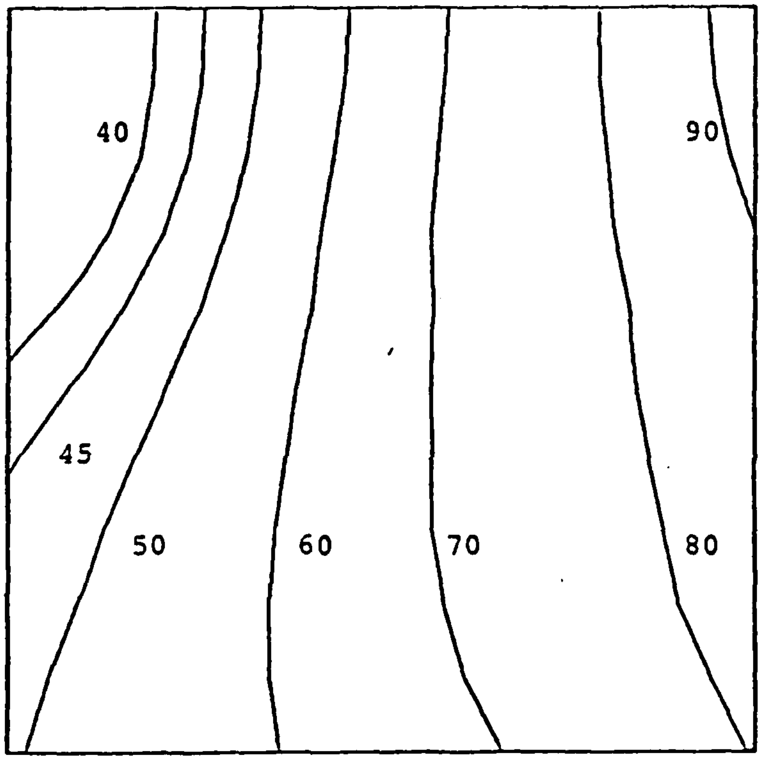

FIG. 10c. VELOCITY CONTOURS AT $\theta = 60°$.

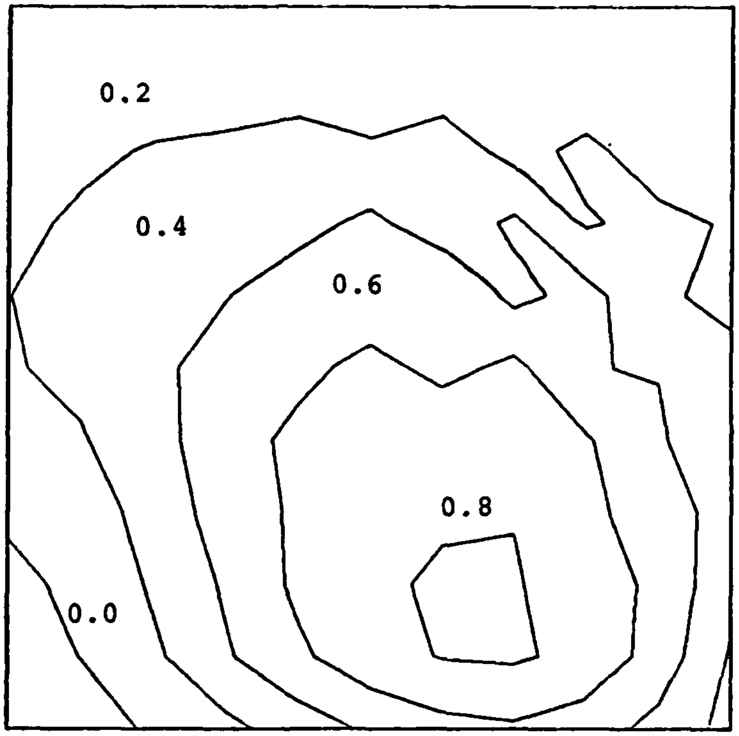

FIG. 11A. SECONDARY VORTICITY, θ = 90°.

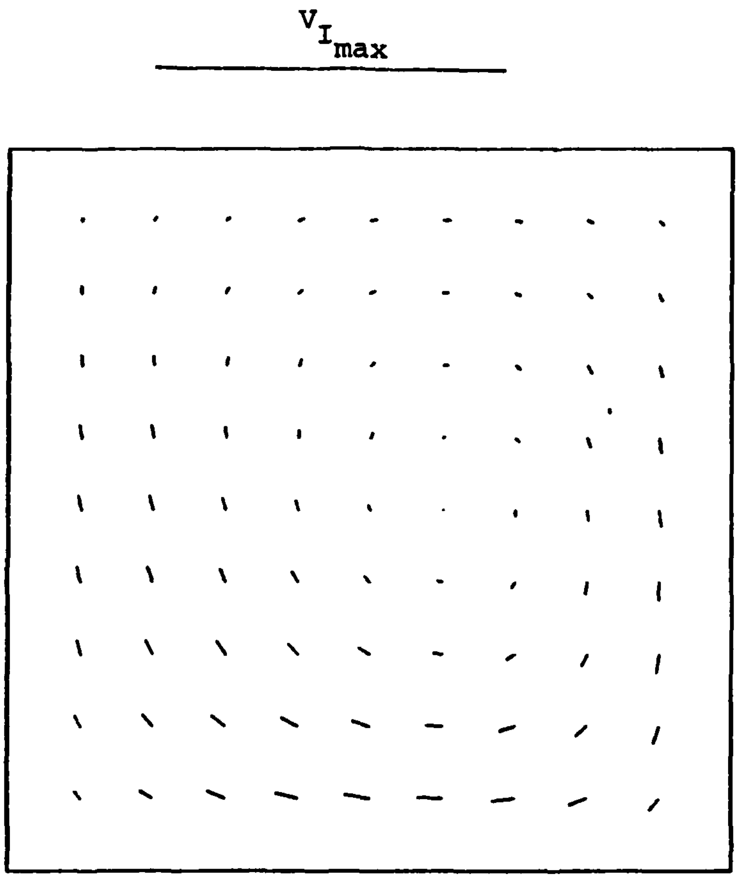

FIG. 11B. SECONDARY VELOCITIES, θ = 90°.

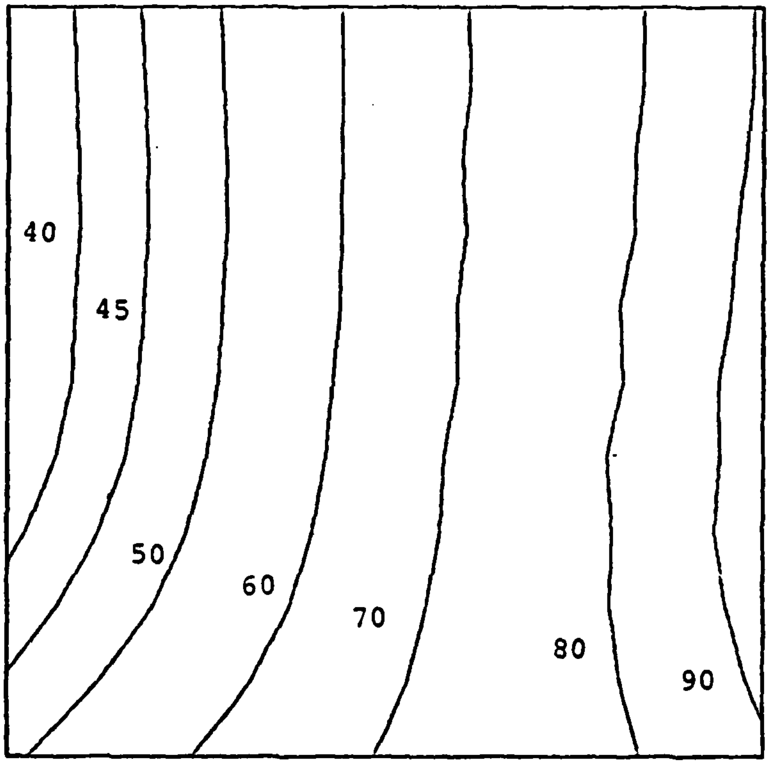

FIG. 11c. VELOCITY CONTOURS AT θ = 90°.

DAT
FILM